A Photometric Study of Five Low Mass Contact Binaries

Edward J. Michaels
Stephen F. Austin State University, Department of Physics, Engineering and Astronomy, P.O. Box 13044, Nacogdoches, TX 75962; emichaels@sfasu.edu

Received August 16, 2019; revised September 1, 2019; accepted September 1, 2019

Abstract Presented are precision multicolor photometry and the results of light curve modeling for five recently discovered contact binary systems: V338 Dra, NSVS 6133550, V1377 Tau, NSVS 3917713, and V2802 Ori. These systems all have orbital periods of less than 0.3 d and stellar effective temperatures less than solar. The photometric solutions derived from the Wilson-Devinney program resulted in contact configurations for each system. The solution mass ratios should be well determined since the light curves of each system exhibited total eclipses. A reliable mass ratio allowed absolute parameters of the component stars to be estimated. Light curve asymmetries were apparent in all five stars. These were attributed to magnetic activity and were modeled as cool and hot spots on the stars.

1. Introduction

1.1. Background

W UMa contact binaries are surprisingly common in the solar neighborhood. Recent surveys have discovered many new candidates in this W-subtype group (ASAS, Pojmański 1997; NSVS, Woźniak *et al.* 2004; CRTS, Drake *et al.* 2014). Most of these candidates have not received follow-up photometric studies. A number of these eclipsing systems were placed on an observing program at the Waffelow Creek Observatory to obtain precision multi-band CCD photometry. Several studies have already been completed: BN Ari, PY Boo, V958 Mon, V2790 Ori, V737 Cep, and V384 Ser (Michaels 2015, 2016a, 2016b, 2016c, 2018; Michaels *et al.* 2019). These stars are all low mass contact binaries (LMCB) with orbital periods of less than 0.3 d.

Presented in this paper are the results from recent photometric observations for five additional LMCB. A brief history of each system is given in the next subsection, with the photometric observations presented in section 2. New minima times, ephemerides, observed properties of each system, and analysis of the light curves using the Wilson-Devinney model are presented in section 3. Discussion of the results and conclusions are given in section 4.

1.2. Notes on individual stars

V338 Dra Khruslov (2006) identified V338 Dra (GSC 04182-01259, 2MASS J15491114+6038029) as a W-subtype eclipsing binary from The Northern Sky Variability (NSVS) data base. It was also classified as a W-subtype by Hoffman *et al.* (2009) using NSVS and by Drake *et al.* (2014) using data from the Catalina Real-time Transient Survey (CRTS). Two times of minima and light elements were published by Hoňková *et al.* (2013) who gives an orbital period of P = 0.235149 d. A third minima time is given by Hübscher and Lehmann (2015). Using all-sky spectrally matched Tycho-2 stars, Pickles and Depagne (2010) found a spectral type of K4V.

NSVS 6133550 Located in the constellation Lacerta, NSVS 6133550 (GSC 03223-01180, TYC 3223-1180-1) was first identified as a variable star in the NSVS survey (Woźniak *et al.* 2004). It was classified as a W-type eclipsing binary in Gettel *et al.*'s (2006) catalogue of 1,022 bright contact binaries which gives an orbital period of 0.27511 d. This star is also listed as a contact binary in a number of additional catalogues (Hoffman *et al.* 2009; Terrell *et al.* 2012; Drake *et al.* 2014). McDonald *et al.* (2017) give an effective temperature of T_{eff} = 5467K and Ammons *et al.* (2006) give a similar value of T_{eff} = 5474 K. Using all-sky spectrally matched Tycho-2 stars, Pickles and Depagne (2010) determined a spectral type of K0V. Only two light minima were found in the literature for this star (Hübscher and Lehmann 2013).

V1377 Tau The variability of V1377 Tau (GSC 00067-00348, ASAS J033959+0314.5) was identified in the All-Sky Automated Survey (ASAS) and was classified as a contact eclipsing system (EC) with an orbital period of P = 0.282709 d. Automated variable star classification techniques using NSVS and ASAS observations also classified it as a W UMa close contact binary (Hoffman *et al.* 2009; Richards *et al.* 2012). Data from the ROSAT X-ray satellite indicates this star is an X-ray source (Appenzeller *et al.* 1998; Szczygiel *et al.* 2008). In a study of ROSAT late-type stars, the spectral type and distance to V1377 Tau were determined. Using medium and high-resolution spectroscopy gives a spectral type of K2, a distance of 194 pc, and a rotational velocity of 63 km/s for the primary star (Zickgraf *et al.* 2005). A total of eight light minima were found in the literature (Diethelm 2010, 2012; Nagai 2012).

NSVS 3917713 NSVS 3917713 (GSC 03280-00990, 2MASS J01541484+4618008) is located in the constellation of Andromeda. It was discovered in the NSVS survey data and classified as an EW-type binary star with an orbital period of P = 0.289222 d and has a maximum V magnitude of 13.087 (Gettel *et al.* 2006). It was also identified as a contact binary by Hoffman *et al.* (2009). Observations of this star were acquired by the All-Sky Automated Survey for Supernovae (ASAS-SN; Kochanek *et al.* 2017) and by SuperWASP (Butters *et al.* 2010). Light curves from these data are also indicative of a contact binary. A literature search did not locate any minima times for this star.

V2802 Ori V2802 Ori (GSC 00103-00894, TYC 103-894-1) was first identified as a variable star in the ASAS survey (Pojmański 1997). It is listed in the fifth part of their *Catalog of Variable Stars* which gives a period of 0.295706 d, a visual

magnitude of V = 11.25, and a ΔV = 0.70 (Pojmański *et al.* 2002). An NSVS automated classification technique identified this star as a W UMa contact binary (Hoffman *et al.* 2009). Pilecki and Stępień (2012) performed light curve modeling on this star using ASAS data.

2. Photometric observations

Multi-band photometric observations for all stars were acquired using a 0.36-m Ritchey-Chrétien robotic telescope at the Waffelow Creek Observatory (http://obs.ejmj.net/index.php). All images were acquired using a SBIG-STXL camera equipped with a cooled KAF-6303E CCD (–30° C). The telescope and camera have an image scale of 0.65 arcsec / pixel and a field of view 33.7' × 22.5'. Each star was imaged in three passbands, Sloan g', r', and i'. In addition, observations in the Johnson B and V passbands were obtained for NSVS 6133550 and Johnson V for V2802 Ori. The observation season, number of images acquired, and the number of nights needed to complete the multi-color light curves are given in Table 1. Bias, dark, and flat frames were obtained on each night for image calibration. MIRA software (Mirametrics 2015) was used for image calibration and to perform the ensemble differential aperture photometry of the light images. The finder charts, Figures 1–5, show the locations of the comparison and check stars, which should be useful for future observers. Table 2 lists the comparison and check stars and their standard magnitudes taken from the AAVSO Photometric All-Sky Survey data base (APASS; Henden *et al.* 2015). The instrumental magnitudes for each star were converted to standard magnitudes using these calibrated comparison star magnitudes. The Heliocentric Julian Date of each observation was converted to orbital phase (φ) using the new epochs and orbital periods given in Table 5. The folded light curves for each star are shown in Figures 6–10. All light curves in this paper were plotted from orbital phase –0.6 to 0.6 with negative phase defined as φ – 1. Error bars were omitted from the plotted points for clarity. The Sloan r' check-star magnitudes are plotted on the bottom panel of Figures 6–10. The check-star magnitudes were plotted and inspected each night, but no significant variability was found. The standard deviations for all check star observations are in Table 2. The standard error of a single observation ranged from 5 to 10 mmag. The light curve properties for each star are given in Table 3 (Min I, Min II, Max I, Max II, Δm, and total eclipse duration). The observations for each star can be accessed from the AAVSO International Database (Kafka 2017).

3. Analysis

3.1. Ephemerides

New times of minima for each star were determined using the Kwee and van Woerden (1956) method. These minima and other minima found in the literature are compiled in Table 4. For each star, the initial epoch was taken from the first primary minimum listed in Table 4 and the orbital period from The International Variable Star Index (VSX, Watson *et al.* 2006–2014). These light elements are shown in Table 5 and were used to calculate the (O–C) residuals in Table 4. Table 5 also gives new linear elements computed by least-squares solution using these residuals.

3.2. Color, temperature, spectral type, absolute magnitude, luminosity

For all systems in this paper the primary star is the hotter and lower mass component of each binary. The spectral type of V1377 Tau was determined from medium and high-resolution spectroscopy (Zickgraf *et al.* 2005). Its K2 spectral type gives an effective temperature of $T_{eff} = 5080 \pm 200$ K (Pecaut and Mamajek 2013). The effective temperatures of the other stars were determined from the average of their observed colors. To find the observed color, the phase and magnitude of the g' and r' observations were binned with a phase width of 0.01. The phases and magnitudes in each bin interval were averaged. The binned r' magnitudes were subtracted from the linearly interpolated g' magnitudes, resulting in an observed (g'–r') color at each phase point. Figure 11 shows the binned Sloan r' light curve of V338 Dra with the (g'–r') color plot in the bottom panel. All five systems show only small color changes over their entire orbital phase range due to the small temperature differences between the component stars. The observed colors were corrected for color excess using three-dimensional maps of interstellar dust reddening based on Pan-STARRS 1 and 2MASS photometry and Gaia parallaxes (Green *et al.* 2018; Gaia 2016, 2018). The color excesses for these stars were very small, which is likely due to their proximity to Earth and their locations above or below the galactic plane. Using the corrected colors, the effective temperature of each star was interpolated from tables of Covey *et al.* (2007) and Pecaut and Mamajek (2013). The resulting average observed colors, color excesses, effective temperatures and spectral types are shown in Table 6. The absolute visual magnitude (M_V) of each star was computed using the following equation:

$$M_V = V - A_V - 5 \log (d / 10), \quad (1)$$

where V is the apparent magnitude at quadrature (φ = 0.75), A_V is the extinction (E(B–V) × 3.086), and d the distance in parsecs. For the stars without B and V observations, the (B–V) color was determined from the transformation equation of Bilir *et al.* (2005):

$$B - V = \frac{(g' - r') + 0.25187}{1.12431}, \quad (2)$$

and the V magnitude from the transformation equation of Jester *et al.* (2005):

$$V = g' - 0.59 (g' - r') - 0.01. \quad (3)$$

The distances in parsecs were determined from Gaia DR2 parallaxes (Bailer-Jones *et al.* 2018; Gaia 2016, 2018). The luminosity of each star in solar units can now be determined using the following equation:

$$M_V + BC_V = 4.74 - 2.5 \log (L / L_\odot), \quad (4)$$

where BC_V is the star's bolometric correction as interpolated

Table 1. Observation log.

System	*Dates*	*No. Nights*	*Images Acquired*				
			B	*V*	*Sloan g′*	*Sloan r′*	*Sloan i′*
V338 Dra	2017 May/Jun	8	—	—	690	626	669
NSVS 6133550	2017 Sep	9	764	1355	700	691	684
V1377 Tau	2017 Nov	4	—	—	388	444	449
NSVS 3917713	2017 Oct	8	—	—	734	1256	1336
V2802 Ori	2017 Dec	4	—	625	553	716	570

Table 2. APASS comparison and check star magnitudes.

System	*R.A. (2000)* *h*	*Dec (2000)* °	*B*	*V*	*g′*	*r′*	*i′*
V338 Dra	15.81976	+60.63414					
GSC 04182-01005 (C1)	15.84121	+60.78514	—	—	12.633	12.279	12.191
GSC 04182-00409 (C2)	15.82763	+60.79534	—	—	13.127	12.657	12.499
GSC 04182-00968 (C3)	15.79748	+60.79923	—	—	13.461	12.716	12.430
GSC 04182-01121 (C4)	15.80262	+60.57336	—	—	14.011	13.501	13.293
GSC 04182-00793 (C5)	15.82888	+60.72875	—	—	14.197	13.760	13.597
GSC 04182-01317 (C6)	15.85001	+60.70778	—	—	14.230	13.638	13.430
GSC 04182-00069 (K)	15.83814	+60.53532	—	—	13.675	13.400	13.315
Standard deviation of observed K-star magnitudes					± 0.011	± 0.009	± 0.011
NSVS 6133550	22.92147	+42.27613					
GSC 03223-01990 (C1)	22.93187	+42.31625	11.954	11.427	11.667	11.314	11.229
GSC 03223-01816 (C2)	22.93552	+42.15188	12.533	12.014	12.224	11.895	11.753
GSC 03223-01366 (C3)	22.92861	+42.24221	13.032	12.411	12.701	12.257	12.115
GSC 03223-01720 (C4)	22.92168	+42.41160	13.232	12.669	12.979	12.513	12.372
GSC 03223-02743 (C5)	22.93296	+42.24837	12.438	11.307	11.858	10.968	10.621
GSC 03223-01801 (C6)	22.90797	+42.30702	13.069	12.526	12.742	12.436	12.338
GSC 03223-03029 (C7)	22.93831	+42.21739	13.045	12.285	12.644	12.086	11.913
GSC 03223-03377 (K)	22.93798	+42.14120	13.251	11.859	12.517	11.430	10.945
Standard deviation of observed K-star magnitudes			± 0.016	± 0.008	± 0.010	± 0.007	± 0.008
V1377 Tau	3.66640	+3.24181					
GSC 00068-00333 (C1)	3.67456	+3.21767	—	—	13.189	12.789	12.666
GSC 00068-00903 (C2)	3.67394	+3.38703	—	—	12.842	12.413	12.284
GSC 00068-00029 (C3)	3.67622	+3.13630	—	—	13.248	12.757	12.570
TYC 67-331-1 (K)	3.65294	+3.10299	—	—	12.008	11.517	11.507
Standard deviation of observed K-star magnitudes					± 0.005	± 0.005	± 0.005
NSVS 3917713	1.90413	+46.30014					
GSC 03280-00679 (C1)	1.89989	+46.29019	—	—	13.633	12.943	12.621
GSC 03280-00905 (C2)	1.91095	+46.25715	—	—	13.113	12.574	12.370
GSC 03280-00996 (C3)	1.90056	+46.22029	—	—	13.413	12.694	12.421
GSC 03280-01188 (C4)	1.89365	+46.33531	—	—	13.161	12.560	12.340
GSC 03280-00594 (C5)	1.90456	+46.38871	—	—	13.912	12.971	12.548
GSC 03280-00799 (C6)	1.89889	+46.20799	—	—	13.114	12.294	11.974
GSC 03280-01340 (C7)	1.91112	+46.40029	—	—	13.799	13.241	13.031
GSC 03280-00987 (K)	1.89692	+46.21784	—	—	13.164	12.755	12.611
Standard deviation of observed K-star magnitudes					± 0.006	± 0.007	± 0.007
V2802 Ori	5.14771	+2.82089					
GSC 00103-00935 (C1)	5.14937	+2.84725	—	12.039	12.252	11.911	11.840
GSC 00103-01035 (C2)	5.15145	+2.85907	—	11.976	12.473	11.590	11.278
GSC 00103-00635 (C3)	5.15774	+2.76971	—	12.044	12.230	11.908	11.871
GSC 00103-01151 (C4)	5.14075	+2.70028	—	12.078	12.310	11.926	11.812
GSC 00103-00761 (K)	5.15299	+2.89693	—	11.231	11.756	10.827	10.493
Standard deviation of observed K-star magnitudes				± 0.005	± 0.006	± 0.006	± 0.006

Table 3. Average light curve properties.

System		Min I Mag.	Min II Mag.	Max I Mag.	Max II Mag.	Δ Mag. MagMax II – Min I	Total Eclipse Duration (minutes)
V338 Dra	g'	14.71 ± 0.03	14.71 ± 0.02	14.00 ± 0.02	13.92 ± 0.02	0.79 ± 0.03	≈ 10
	r'	13.75 ± 0.01	13.74 ± 0.01	13.09 ± 0.03	13.04 ± 0.03	0.71 ± 0.04	—
	i'	13.33 ± 0.02	13.33 ± 0.02	12.70 ± 0.05	12.67 ± 0.05	0.66 ± 0.06	—
NSVS 6133550	B	12.51 ± 0.01	12.48 ± 0.01	12.05 ± 0.01	12.03 ± 0.01	0.49 ± 0.02	≈20
	V	11.74 ± 0.01	11.72 ± 0.01	11.32 ± 0.01	11.28 ± 0.01	0.46 ± 0.01	—
	g'	12.11 ± 0.01	12.08 ± 0.01	11.67 ± 0.02	11.64 ± 0.02	0.48 ± 0.02	—
	r'	11.53 ± 0.01	11.50 ± 0.01	11.11 ± 0.01	11.08 ± 0.01	0.45 ± 0.01	—
	i'	11.31 ± 0.01	11.28 ± 0.01	10.91 ± 0.02	10.88 ± 0.02	0.43 ± 0.02	—
V1377 Tau	g'	12.55 ± 0.01	12.45 ± 0.01	11.70 ± 0.02	11.66 ± 0.02	0.89 ± 0.02	≈12
	r'	11.79 ± 0.01	11.71 ± 0.01	10.97 ± 0.01	10.97 ± 0.01	0.83 ± 0.02	—
	i'	11.53 ± 0.01	11.46 ± 0.01	10.75 ± 0.01	10.72 ± 0.01	0.81 ± 0.01	—
NSVS 3917713	g'	14.02 ± 0.02	14.06 ± 0.01	13.41 ± 0.01	13.41 ±0.01	0.61 ± 0.02	≈21
	r'	13.35 ± 0.02	13.38 ± 0.01	12.77 ± 0.02	12.77 ± 0.02	0.58 ± 0.02	—
	i'	13.07 ± 0.02	13.08 ± 0.01	12.51 ± 0.02	12.50 ± 0.02	0.57 ± 0.03	—
V2802 Ori	V	11.80 ± 0.01	11.75 ± 0.01	11.19 ± 0.02	11.17 ± 0.02	0.63 ± 0.02	≈25
	g'	12.15 ± 0.01	12.10 ± 0.01	11.52 ± 0.02	11.50 ± 0.02	0.65 ± 0.02	—
	r'	11.53 ± 0.01	11.47 ± 0.01	10.93 ± 0.02	10.91 ± 0.02	0.61 ± 0.02	—
	i'	11.32 ± 0.01	11.27 ± 0.01	10.74 ± 0.02	10.73 ± 0.02	0.59 ± 0.02	—

from the tables of Pecaut and Mamajek (2013). Each systems absolute and apparent visual magnitudes at quadrature, stellar distance, and observed luminosity are shown in Table 6.

3.3. Light curve modeling

For light curve modeling, the standard magnitudes were binned in both phase and magnitude as detailed in section 3.2. The resulting binned magnitudes were converted to relative flux units. The first step employed in modeling each star was to attain preliminary fits to the observed light curves using the program BINARYMAKER3.0 (BM3; Bradstreet and Steelman 2002). Standard convective parameters were employed in the model, with the limb darkening coefficients taken from van Hamme's (1993) tabular values. The asymmetries in the light curves were not modeled initially with BM3. Once a good fit was obtained between the synthetic and observed light curves, the resulting parameters for each passband were averaged. These values were used as the input parameters for the Wilson-Devinney (WD) program where computations were done simultaneously in all passbands (Wilson and Devinney 1971; van Hamme and Wilson 1998). The light curve morphology of each star indicates a contact configuration, with the stars having a common convective envelope. The WD program was configured for overcontact binaries (Mode 3) and the Kurucz stellar atmosphere model was applied (Kurucz 2002). Each binned input data point was assigned a weight equal to the number of observations forming that point. The fixed inputs included standard convective parameters: gravity darkening, $g_1 = g_2 = 0.32$ (Lucy 1968) and albedo value $A_1 = A_2 = 0.5$ (Ruciński 1969). The temperature of the primary stars, T_1, were fixed at values given in Table 6 (see section 3.2). Logarithmic limb darkening coefficients were calculated by the program from tabulated values using the method of van Hamme (1993). The solution's adjustable parameters include the inclination (i), mass ratio ($q = M_2 / M_1$), potential ($\Omega_1 = \Omega_2$), temperature of the secondary star (T_2), the normalized flux for each wavelength (L), third light (l), and phase shift.

Low mass, rapidly revolving contact binaries are often magnetically active and thus spotted. Except for NSVS 3917713, the light curves for each star show an O'Connell effect with Max II ($\varphi = 0.75$) brighter than Max I ($\varphi = 0.25$), which is indicative of spotting (O'Connell 1951). In addition, the primary total eclipses of NSVS 6133550 and V2802 Ori are not flat, but having a small but obvious slope, which is also likely caused by star spots. Once the initial WD solutions were obtained, the resulting parameter values were transferred into BM3 to model the asymmetries in the light curves caused by star spots. Four of the stars required one or two cool spots on the larger secondary star to minimize the asymmetries. A single hot spot on the primary star of NSVS 3917713 provided the best fit. Two systems, NSVS 6133550 and NSVS 3917713, required a small third light (l) to fit the minima. The resulting best-fit BM3 parameters were then incorporated into new WD solutions that included adjustable spot parameters (co-latitude, longitude, radius, and temperature factor). The final spotted WD solution parameters for each star are shown in Table 7. The filling factor in Table 7 was computed using the method of Lucy and Wilson (1979) given by:

$$f = \frac{\Omega_{inner} - \Omega}{\Omega_{inner} - \Omega_{outer}}, \quad (5)$$

where Ω_{inner} and Ω_{outer} are the inner and outer critical equipotential surfaces and Ω is the equipotential that describes the stellar surface. Figures 12–16 show the normalized light curves overlaid by the synthetic solution curves (solid line), with the residuals shown in the bottom panel. A BM3 graphical representation of each system solution is shown in Figure 17 (Bradstreet and Steelman 2002).

Table 4. Times of minima and O-C residuals.

Epoch HJD 2400000+	*Error*	*Cycle*	*O-C*	*References*
V338 Dra				
56421.36484	0.00007	0.0	0.00000	Hoňková 2013
56421.48221	0.00005	0.5	–0.00020	Hoňková 2013
56771.50050	0.00630	1489.0	–0.00120	Hübscher and Lehman 2015
57888.69135	0.00007	6240.0	–0.00325	present paper
57888.80810	0.00006	6240.5	–0.00408	present paper
57898.68440	0.00007	6282.5	–0.00404	present paper
57898.80270	0.00005	6283.0	–0.00331	present paper
57899.74390	0.00007	6287.0	–0.00271	present paper
57911.73590	0.00005	6338.0	–0.00331	present paper
57911.85280	0.00005	6338.5	–0.00398	present paper
57912.67650	0.00006	6342.0	–0.00330	present paper
57912.79340	0.00006	6342.5	–0.00398	present paper
57913.73390	0.00007	6346.5	–0.00407	present paper
57913.85241	0.00008	6347.0	–0.00314	present paper
57915.73370	0.00006	6355.0	–0.00304	present paper
57915.85030	0.00007	6355.5	–0.00401	present paper
NSVS 6133550				
56159.42270	0.00100	–0.5	0.00336	Hübscher and Lehman 2013
56159.55690	0.00080	0.0	0.00000	Hübscher and Lehman 2013
58010.66296	0.00027	6728.5	0.00824	present paper
58011.62795	0.00031	6732.0	0.01034	present paper
58011.76341	0.00029	6732.5	0.00824	present paper
58012.72852	0.00029	6736.0	0.01045	present paper
58012.86400	0.00027	6736.5	0.00838	present paper
58013.68921	0.00059	6739.5	0.00825	present paper
58013.82914	0.00028	6740.0	0.01062	present paper
58015.61510	0.00010	6746.5	0.00835	present paper
58015.75541	0.00011	6747.0	0.01110	present paper
58017.68097	0.00010	6754.0	0.01087	present paper
58019.60753	0.00012	6761.0	0.01164	present paper
58019.74275	0.00012	6761.5	0.00930	present paper
58019.88242	0.00007	6762.0	0.01141	present paper
58020.70756	0.00010	6765.0	0.01122	present paper
58020.84325	0.00007	6765.5	0.00935	present paper
58021.66867	0.00013	6768.5	0.00943	present paper
58021.80829	0.00008	6769.0	0.01149	present paper
V1377 Tau				
55192.55900	0.00030	0.0	0.00000	Diethelm 2010
55544.67420	0.00050	1245.5	0.00114	Diethelm 2010
55568.98700	—	1331.5	0.00097	Nagai 2012
55571.95560	—	1342.0	0.00112	Nagai 2012
55573.93480	—	1349.0	0.00136	Nagai 2012
55574.92300	—	1352.5	0.00008	Nagai 2012
55862.86560	0.00040	2371.0	0.00356	Diethelm 2012
56282.68990	0.00030	3856.0	0.00500	Diethelm 2013
58078.74551	0.00005	10209.0	0.01033	present paper
58078.88644	0.00002	10209.5	0.00990	present paper
58080.72452	0.00009	10216.0	0.01038	present paper
58080.86551	0.00003	10216.5	0.01001	present paper
58081.71352	0.00003	10219.5	0.00989	present paper
58081.85522	0.00003	10220.0	0.01024	present paper
58084.68258	0.00003	10230.0	0.01051	present paper
58084.82341	0.00003	10230.5	0.00999	present paper
NSVS 3917713				
56897.98995	—	–3941.0	–0.00577	Jayasinghe 2018
58037.76839	0.00008	0.0	0.00000	present paper
58037.91343	0.00008	0.5	0.00044	present paper
58038.63572	0.00008	3.0	–0.00030	present paper
58038.78066	0.00008	3.5	0.00004	present paper
58038.92498	0.00007	4.0	–0.00025	present paper
58039.64826	0.00008	6.5	0.00001	present paper
58039.79283	0.00007	7.0	–0.00002	present paper
58039.93739	0.00007	7.5	–0.00007	present paper
58040.66044	0.00007	10.0	–0.00004	present paper
58040.80540	0.00008	10.5	0.00032	present paper
58043.69731	0.00009	20.5	0.00014	present paper
58049.62573	0.00009	41.0	–0.00023	present paper
58049.77078	0.00009	41.5	0.00022	present paper
58049.91507	0.00009	42.0	–0.00010	present paper
58050.63822	0.00007	44.5	0.00003	present paper
58050.78261	0.00007	45.0	–0.00018	present paper
58050.92732	0.00007	45.5	–0.00008	present paper
V2802 Ori				
55526.87930	0.00020	–8690.5	0.01688	Diethelm 2011
55882.90720	0.00040	–7486.5	0.01476	Diethelm 2012
56246.91670	0.00040	–6255.5	0.01017	Diethelm 2013
58096.69541	0.00006	0.0	0.00000	present paper
58096.84306	0.00006	0.5	–0.00020	present paper
58097.87840	0.00006	4.0	0.00017	present paper
58097.73031	0.00007	3.5	–0.00007	present paper
58098.76518	0.00007	7.0	–0.00017	present paper
58100.83534	0.00006	14.0	0.00005	present paper
58100.68708	0.00007	13.5	–0.00036	present paper

4. Discussion and conclusions

Provisional absolute stellar parameters were calculated for each system using the mass ratio and an estimate of the secondary star mass (M_2). The light curves of each system displayed a total primary eclipse, which provided the necessary constrains for an accurate determination of the mass ratios (q) (Wilson 1978; Terrell and Wilson 2005; Hambálek and Pribulla 2013). The secondary star masses were calculated using Gazeas and Stępień (2008) period-mass relation for contact binaries:

$$\log M_2 = (0.755 \pm 0.059) \log P + (0.416 \pm 0.024), \quad (6)$$

where P is the orbital period. The primary star's mass (M_1) was calculated using the solution mass ratio. The separation between the mass centers was then calculated using Kepler's Third Law. Using this semi-major axis value, the WD light curve program (LC) computed the radius and bolometric magnitude of each star. The luminosity of each stellar component was then calculated from the bolometric magnitudes. The values for the absolute stellar parameters in solar units are shown in Table 8. The computed solution luminosities are in good agreement with the observed luminosities to within the margin of errors (see Table 6). A comparison was made between the provisional absolute parameters of these systems and the mass and radius distribution of 112 contact binaries in a study by Gazeas and Stępień (2008, see their Figures 1–3). The geometrical and physical properties for those 112 stars were well determined from both photometric and radial velocity measurements. Two of their plots were reproduced in Figures 18 and 19. Figure 18 shows that the stellar radii derived from the photometric solutions are in good agreement with the period-radius relation

Table 5. Linear elements with errors .

System	Initial Elements		New Elements from Least-squares	
	Epoch (HJD)	P_{orb} (days)	Epoch (HJD)	P_{orb} (days)
V338 Dra	2456421.3648	0.235149	2457915.7332 (3)	0.23514847 (5)
NSVS 6133550	2456159.5569	0.275113	2458021.807 (1)	0.2751142 (2)
V1377 Tau	2455192.5590	0.282709	2458084.6823 (3)	0.28271000 (3)
NSVS 3917713	2458037.7684	0.289209	2458050.7828 (1)	0.28921045 (5)
V2802 Ori	2458096.6954	0.295706	2458100.8351 (3)	0.29570410 (6)

Table 6. Observed color, color excess, effective temperature, spectral type, apparent and absolute visual magnitudes at quadrature, distance and luminosity.

System	(g′–r′)	E(g′–r′)	T_{eff} (K)	SP	m_V	M_V	Dist. (pc)	$L_\odot$
V338 Dra	0.92 ± 0.04	0.01 ± 0.02	4749 ± 63	K3	13.39 ± 0.04	6.17 ± 0.09	274 ± 1	0.41 ± 0.04
NSVS 6133550	0.57 ± 0.02	0.00+0.01	5493 ± 54	G8	11.28 ± 0.01	4.98 ± 0.04	182 ± 2	0.94 ± 0.03
V1377 Tau	0.72 ± 0.02	0.00+0.02	5040 ± 200*	K2	11.24 ± 0.03	5.34 ± 0.06	152 ± 1	0.74 ± 0.09
NSVS 3917713	0.66 ± 0.02	0.04 ± 0.02	5301 ± 122	K0	13.02 ± 0.03	5.14 ± 0.09	359 ± 10	0.85 ± 0.07
V2802 Ori	0.60 ± 0.02	0.00+0.01	5359 ± 109	G9	11.17 ± 0.02	4.97 ± 0.02	174 ± 1	0.98 ± 0.03

**Determined spectroscopically.*

(dashed lines). The dashed line in Figure 19 is a power-law fit to the more massive secondary stars (Gazeas and Stępień 2008). This is very similar to the mass-radius relation for single main-sequence (MS) stars with masses less than 1.8 $M_\odot$ (Gimenez and Zamorano 1985). Figure 19 shows that the massive components of each binary pair in this study are MS stars. The smaller, hotter primary stars of contact binaries do not follow a mass-radius relation but are considerably oversized and over-luminous when compared to MS stars of similar masses.

The final WD solutions gave fill-outs for the stars between 9% and 41%. This is consistent with a contact binary where both primary and secondary stars exceed their critical lobes. These systems are W-subtype eclipsing binaries where the more massive cooler secondary star has a lower surface brightness than its companion. The stars are all cooler than the sun, with spectral types from G8 to K3. There were asymmetries in the light curves of each system due to spotting, which indicates magnetically active stars. This is not unexpected, given the low temperature and rapid rotation of the stars.

V338 Dra has a very short orbital period for a LMCB at 0.235 d (5.64 hours). This period is close to the cut-off of ~0.22 d in the period distribution for contact binaries (Ruciński 1992). The components of this system are in shallow contact with a fill-out of 9%. V338 Dra has the coolest and smallest stars of the five systems in this study and the lowest observed luminosity. Two cool spots were modeled on the larger secondary star to account for the asymmetries in the light curves. The WD solution result showed negligible third light. There are very few contact binaries with orbital periods less than 0.24 d that have well determined physical parameters. RW Com is one of these stars and happens to be remarkably similar to V338 Dra (Deb and Singh 2011). A comparison of the physical and orbital properties of RW Com and V338 Dra is shown in Table 9. Both secondary stars in these systems have masses that are higher than expected, given the temperature and luminosities determined for these main-sequence stars.

The stars of NSVS 6133550 are in moderately deep contact with a fill-out of 41%. The small primary star is about half the radius of its cooler companion. This star has the most extreme mass ratio of the five systems at $q(M_1/M_2) = 0.20$. Light curve asymmetries were modeled by adding two cool spots on the larger cooler component of this magnetically active system. A third light contribution of about 3–4% of the total system flux was necessary to obtain a good fit between the observed and synthetic light curves.

V1377 Tau has a secondary star radius that is only 13% larger than the primary star. The component stars are in shallow contact with a fill-out = 16%. This binary has the deepest primary eclipse of the five systems, with a $\Delta m = 0.89$ in the Sloan g' passband. A single cool spot was modeled on the smaller primary star in the final WD solution iterations. This is the only star in the sample with enough eclipse timings for a preliminary (O–C) period analysis. A least-squares solution using the (O–C) residuals in Table 4 yields the following quadratic ephemeris:

$$\text{HJD Min I} = 2458084.6822(4) + 0.2827095(5)E - 5.6(2) \times 10^{-11} E^2. \quad (7)$$

This ephemeris suggests the orbital period is decreasing at a rate of $dP/dt = -1.4(2) \times 10^{-10}$ d yr^{-1} or 1.2 seconds per century. The quadratic fit to the O–C residuals is shown in Figure 20. Additional eclipse timings will be required to confirm this result.

The stars of the NSVS 3917713 system differ in temperature by about 100 K, giving nearly equal minima depths. These stars may be in thermal equilibrium due to a long evolutionary contact phase. The light curves show little evidence for the O'Connell effect, but a deficit of light was noted after Max II and before Max I. In the final WD iterations, a single hot spot was modeled on the hotter primary star, which greatly improved the fit between the observed and model light curves (residuals four times smaller). This system also required a small third light contribution, about 3% of the total flux, to fit the minima.

V2802 Ori is very similar to NSVS 3917713 in terms of mass ratio, fill-out, and the masses and radii of the individual stars.

Table 7. Results derived from light curve modeling.

Parameter	*V338 Dra*	*NSVS 6133550*	*V1377 Tau*	*NSVS 3917713*	*V2802 Ori*
phase shift	–0.0009 ± 0.0002	–0.0045 ± 0.0003	–0.0019 ± 0.0001	0.0002 ± 0.0001	–0.0024 ± 0.0002
filling factor	9%	41%	16%	21%	18%
i (°)	83.7 ± 0.3	77.6 ± 0.1	87.7 ± 0.8	88.4 ± 1.2	85.1 ± 0.3
T_1 (K)	[1] 4749	[1] 5493	[1] 5040	[1] 5301	[1] 5359
T_2 (K)	4633 ± 28	5267 ± 27	4858 ± 6	5203 ± 4	5068 ± 13
$\Omega_1 = \Omega_2$	5.46 ± 0.03	8.85 ± 0.04	4.85 ± 0.03	6.14 ± 0.02	6.62 ± 0.02
$q(M_2/M_1)$	2.19 ± 0.03	4.96 ± 0.04	1.78 ± 0.02	2.74 ± 0.02	3.09 ± 0.02
$L_1/(L_1+L_2)$ (B)	—	0.2495 ± 0.0037	—	—	—
$L_1/(L_1+L_2)$ (V)	—	0.2369 ± 0.0026	—	—	0.3317 ± 0.0027
$L_1/(L_1+L_2)$ (g')	0.3737 ± 0.0059	0.2438 ± 0.0032	0.4347 ± 0.0028	0.3141 ± 0.0017	0.3427 ± 0.0030
$L_1/(L_1+L_2)$ (r')	0.3597 ± 0.0038	0.2310 ± 0.0021	0.4171 ± 0.0024	0.3073 ± 0.0013	0.3216 ± 0.0024
$L_1/(L_1+L_2)$ (i')	0.3546 ± 0.0031	0.2259 ± 0.0018	0.4099 ± 0.0019	0.3045 ± 0.0011	0.3130 ± 0.0021
l_3 (B)	—	[2] 0.04 ± 0.02	—	—	—
l_3 (V)	—	[2] 0.03 ± 0.02	—	—	—
l_3 (g′)	—	[2] 0.04 ± 0.02	—	[2] 0.035 ± 0.005	—
l_3 (r′)	—	[2] 0.03 ± 0.01	—	[2] 0.018 ± 0.005	—
l_3 (i′)	—	[2] 0.03 ± 0.01	—	[2] 0.017 ± 0.005	—
r_1 side	0.3109 ± 0.0011	0.2551 ± 0.0008	0.3278 ± 0.0009	0.2968 ± 0.0010	0.2854 ± 0.0006
r_2 side	0.4721 ± 0.0051	0.5639 ± 0.0039	0.4525 ± 0.0044	0.4918 ± 0.0030	0.4989 ± 0.0029
Spot Parameters					
Spot 1	$Star_2$	$Star_2$	$Star_2$	$Star_1$	$Star_2$
colatitude (°)	44 ± 15	52 ± 14	123 ± 32	131 ± 8	43 ± 10
longitude (°)	101 ± 4	121 ± 4	122 ± 3	5 ± 1	117 ± 3
spot radius (°)	24 ± 7	26 ± 7	17 ± 9	32 ± 5	20 ± 4
temp. factor	0.86 ± 0.04	0.95 ± 0.03	0.82 ± 0.07	1.11 ± 0.04	0.82 ± 0.03
Spot 2	$Star_2$	$Star_2$			$Star_2$
colatitude (°)	58 ± 11	88 ± 3	—	—	49 ± 9
longitude (°)	356 ± 4	4 ± 1	—	—	325 ± 9
spot radius (°)	20 ± 6	21 ± 3	—	—	15 ± 3
temp. factor	0.90 ± 0.04	0.91 ± 0.03	—	—	0.79 ± 0.05

[1] Assumed. [2] Third lights are the percent of light contributed at orbital phase 0.25. The subscripts 1 and 2 refer to the star being eclipsed at primary and secondary minimum, respectively. Note: The errors in the stellar parameters result from the least–squares fit to the model. The actual uncertainties are considerably larger.

Table 8. Provisional absolute parameters (solar units).

System	*A*	M_1	M_2	R_1	R_2	L_1	L_2	$L_1 + L_2$
V338 Dra	1.74 ± 0.04	0.40 ± 0.04	0.87 ± 0.09	0.56 ± 0.01	0.79 ± 0.02	0.14 ± 0.01	0.26 ± 0.03	0.40 ± 0.04
NSVS 6133550	1.88 ± 0.05	0.20 ± 0.02	0.98 ± 0.09	0.51 ± 0.01	1.02 ± 0.03	0.22 ± 0.01	0.72 ± 0.06	0.93 ± 0.08
V1377 Tau	2.10 ± 0.05	0.56 ± 0.05	1.00 ± 0.09	0.72 ± 0.02	0.93 ± 0.02	0.30 ± 0.06	0.43 ± 0.13	0.73 ± 0.18
NSVS 3917713	2.06 ± 0.05	0.37 ± 0.03	1.02 ± 0.09	0.64 ± 0.01	0.99 ± 0.03	0.29 ± 0.03	0.65 ± 0.10	0.94 ± 0.14
V2802 Ori	2.08 ± 0.05	0.34 ± 0.03	1.04 ± 0.09	0.62 ± 0.01	1.02 ± 0.03	0.28 ± 0.03	0.62 ± 0.08	0.90 ± 0.11

Note: The calculated values in this table are provisional. Radial velocity observations are not available for direct determination of M_1, M_2, and a.

Table 9. Comparison of physical and orbital parameters (solar units).

Star	*P (day)*	*A*	M_1	M_2	R_1	R_2	T_1 *(K)*	T_2 *(K)*	L_1	L_2
RW Com	0.2373	1.72	0.39	0.83	0.56	0.79	4830	4517	0.15	0.23
V338 Dra	0.2351	1.74	0.40	0.87	0.56	0.79	4749	4633	0.14	0.26

The photometric solution values for V2802 Ori, inclination, temperature ratio (T_2/T_1), and mass ratio (i = 85.1°, $T_2/T_1 = 0.98$, q = 3.09) were in good agreement with light curve modeling using ASAS survey data (i = 83.5°, $T_2/T_1 = 0.94$, q = 2.86) (Pilecki and Stepień 2012).

Evolutionary models of LMCB indicate these systems should be undergoing mass transfer from the currently less massive star to their companions (Stępień 2006, 2011). This would result in the lengthening of their orbital periods. Concurrently, angular momentum and mass loss due to magnetized winds would have the opposite effect, decreasing the orbital period. The angular momentum loss (AML) should dominate in LMCB, causing the orbits to contract, and eventually leading to the binary overflowing their outer critical surface. The binary would then merge, forming a single, rapidly rotating star. The extreme mass ratio of NSVS 6133550 was likely the result of this evolutionary driven combination of mass transfer and AML. Except for V1377 Tau, the eclipse timings currently available for these stars are few. Determining whether these stars are undergoing secular period changes will require additional observations. Cyclic variations in the period are also possible due to an orbiting third body. The third light modeled in the WD solutions for NSVS 6133550 and NSVS 3017713 could be the result of a low mass third star in these two systems. New eclipse timings over many years may provide evidence to support this supposition. In addition, a spectroscopic study of these systems would also be invaluable to confirming the provisional absolute stellar parameters presented here.

5. Acknowledgements

This research was made possible through the use of the AAVSO Photometric All-Sky Survey (APASS), funded by the Robert Martin Ayers Sciences Fund. This research has made use of the SIMBAD database and the VizieR catalogue access tool, operated at CDS, Strasbourg, France. This work has made use of data from the European Space Agency (ESA) mission Gaia (https://www.cosmos.esa.int/gaia), processed by the Gaia Data Processing and Analysis Consortium (DPAC, https://www.cosmos.esa.int/web/gaia/dpac/consortium). Funding for the DPAC has been provided by national institutions, in particular the institutions participating in the Gaia Multilateral Agreement. This paper makes use of data from the first public release of the WASP data (Butters *et al.* 2010) as provided by the WASP consortium and services at the NASA Exoplanet Archive, which is operated by the California Institute of Technology, under contract with the National Aeronautics and Space Administration under the Exoplanet Exploration Program.

References

Ammons, S. M., Robinson, S. E., Strader, J., Laughlin, G., Fischer, D., and Wolf, A. 2006, *Astrophys. J.*, **638**, 1004.

Appenzeller, I., *et al.* 1998, *Astrophys. J., Suppl. Ser.*, **117**, 319.

Bailer-Jones, C. A. L., Rybizki, J., Fouesneau, M., Mantelet, G., and Andrae, R. 2018, *Astron. J.*, **156**, 58.

Bilir, S. Karaali, S., and Tunçel, S. 2005, *Astron. Nachr.*, **326**, 321.

Bradstreet, D. H., and Steelman, D. P. 2002, *Bull. Amer. Astron. Soc.*, **34**, 1224.

Butters, O. W., *et al.* 2010, *Astron. Astrophys.*, **520**, L10.

Covey, K. R., *et al.* 2007, *Astron. J.*, **134**, 2398.

Deb, S., and Singh, H. P. 2011, *Mon. Not. Roy. Astron. Soc.*, **412**, 1787.

Diethelm, R. 2010, *Inf. Bull. Var. Stars*, No. 5920, 1.

Diethelm, R. 2011, *Inf. Bull. Var. Stars*, No. 5960, 1.

Diethelm, R. 2012, *Inf. Bull. Var. Stars*, No. 6011, 1.

Diethelm, R. 2013, *Inf. Bull. Var. Stars*, No. 6042, 1.

Drake, A. J., *et al.* 2014, *Astrophys. J., Suppl. Ser.*, **213**, 9.

Gaia Collaboration, *et al.* 2016, *Astron. Astrophys.*, **595A**, 1.

Gaia Collaboration, *et al.* 2018, *Astron. Astrophys.*, **616A**, 1.

Gazeas, K., and Stępień, K. 2008, *Mon. Not. Roy. Astron. Soc.*, **390**, 1577.

Gettel, S. J., Geske, M. T., and McKay, T. A. 2006, *Astron. J.*, **131**, 621.

Gimenez A., and Zamorano J. 1985, *Astrophys. Space Sci.*, **114**, 259.

Green, G. M., *et al.* 2018, *Mon. Not. Roy. Astron. Soc.*, **478**, 651.

Hambálek L., and Pribulla, T. 2013, *Contrib. Astron. Obs. Skalnaté Pleso*, **43**, 27.

Henden, A. A., *et al.* 2015, AAVSO Photometric All-Sky Survey, data release 9, (https://www.aavso.org/apass).

Hoffman, D., Harrison, T. E., and McNamara, B. J. 2009, *Astron. J.*, **138**, 466.

Hoňková, K., *et al.* 2013, *Open Eur. J. Var. Stars*, **160**, 1.

Hübscher, J., and Lehmann, P. B. 2013, *Inf. Bull. Var. Stars*, No. 6070, 1.

Hübscher, J., and Lehmann, P. B. 2015, *Inf. Bull. Var. Stars*, No. 6149, 1.

Jayasinghe, K., *et al.* 2018, *Mon. Not. Roy. Astron. Soc.*, **477**, 3145.

Jester, S., *et al.* 2005, *Astron. J.*, **130**, 873.

Kafka, S. 2017, variable star observations from the AAVSO International Database (https://www.aavso.org/aavso-international-database).

Khruslov, A. V. 2006, *Perem. Zvezdy Prilozh.*, **6**, 16 (http://www.astronet.ru/db/varstars/msg/eid/PZP-06-0016).

Kochanek, C. S., *et al.* 2017, *Publ. Astron. Soc. Pacific*, **129**, 104502.

Kurucz, R. L. 2002, *Baltic Astron.*, **11**, 101.

Kwee, K. K., and van Woerden, H. 1956, *Bull. Astron. Inst. Netherlands*, **12**, 327.

Lucy, L. B. 1968, *Astrophys. J.*, **151**, 1123.

Lucy, L. B., and Wilson, R. E. 1979, *Astrophys. J.*, **231**, 502.

Michaels, E. J. 2015, *J. Amer. Assoc. Var. Star Obs.*, **43**, 231.

Michaels, E. J. 2016a, *J. Amer. Assoc. Var. Star Obs.*, **44**, 30.

Michaels, E. J. 2016b, *J. Amer. Assoc. Var. Star Obs.*, **44**, 53.

Michaels, E. J. 2016c, *J. Amer. Assoc. Var. Star Obs.*, **44**, 137.

Michaels, E. J. 2018, *J. Amer. Assoc. Var. Star Obs.*, **46**, 27.

Michaels, E. J., Lanning, C. M., and Self, S. N. 2019, *J. Amer. Assoc. Var. Star Obs.*, **47**, 43.

McDonald I., Zijlstra, A. A., and Watson, R. A. 2017, *Mon. Not. Roy. Astron. Soc.*, **471**, 770.

Mirametrics. 2015, Image Processing, Visualization, Data Analysis, (https://www.mirametrics.com).

Nagai, K. 2012, *Bull. Var. Star Obs. League Japan*, **53**, 1.
O'Connell, D. J. K. 1951, *Publ. Riverview Coll. Obs.*, **2**, 85.
Pecaut, M. J., and Mamajek, E. E. 2013, *Astrophys. J., Suppl. Ser.*, **208**, 9 (http://www.pas.rochester.edu/~emamajek/EEM_dwarf_UBVIJHK_colors_Teff.txt).
Pickles, A., and Depagne, E. 2010, *Publ. Astron. Soc. Pacific*, **122**, 1437.
Pilecki, B., and Stępień, K. 2012, *Inf. Bull. Var. Stars*, No. 6012, 1.
Pojmański, G. 1997, *Acta Astron.*, **47**, 467.
Pojmański, G. *et al.* 2002, *Acta Astron.*, **52**, 397.
Richards, J. W., Starr, D. L., Miller, A. A., Bloom, J. S., Butler, N. R., Brink, H., and Crellin-Quick, A. 2012, *Astrophys. J., Suppl. Ser.*, **203**, 32.
Ruciński, S. M. 1969, *Acta Astron.*, **19**, 245.
Ruciński, S. M. 1992, *Astron. J.*, **103**, 960.
Stępień, K., 2006, *Acta Astron.*, **56**, 199.
Stępień, K., 2011, *Acta Astron.*, **61**, 139.
Szczygiel, D. M., Socrates, A., Paczyński, B., Pojmański, G., and Pilecki, B. 2008, *Acta Astron.*, **58**, 405.
Terrell, D., Gross, J., and Cooney, W. R. 2012, *Astron. J.*, **143**, 99.
Terrell, D., and Wilson, R. E. 2005, *Astrophys. Space Sci.*, **296**, 221.
van Hamme, W. 1993, *Astron. J.*, **106**, 2096.
van Hamme, W., and Wilson, R. E. 1998, *Bull. Amer. Astron. Soc.*, **30**, 1402.
Watson, C., Henden, A. A., and Price, C. A. 2014, AAVSO International Variable Star Index VSX (Watson+, 2006–2014, http://www.aavso.org/vsx).
Wilson, R. E. 1978, *Astrophys. J.*, **224**, 885.
Wilson, R. E., and Devinney, E. J. 1971, *Astrophys. J.*, **166**, 605.
Woźniak, P. R., *et al.* 2004, *Astron. J.*, **127**, 2436.
Zickgraf, J., Krautter, J., Reffert, S., Alcalá, J. M., Mujica, R., Covino, E., and Sterzik, M. F. 2005, *Astron. Astrophys.*, 433, 151.

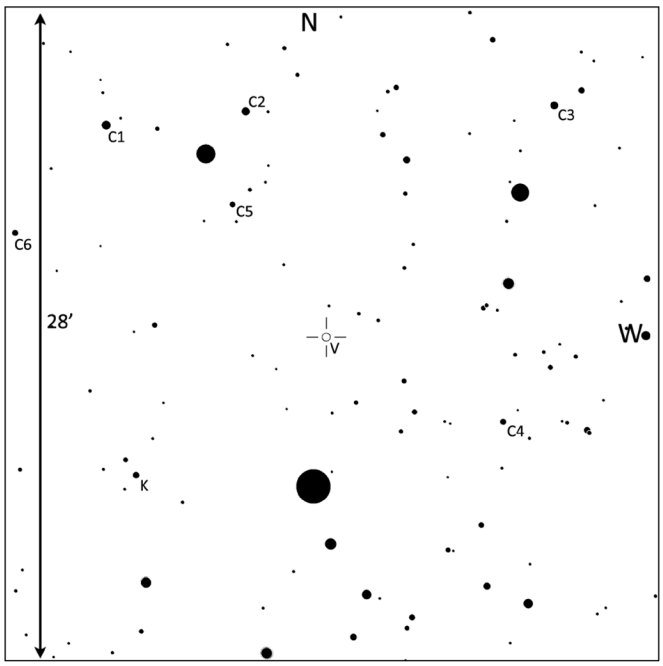

Figure 1. Finder chart for V338 Dra (V), comparison (C1–C6), and check (K) stars.

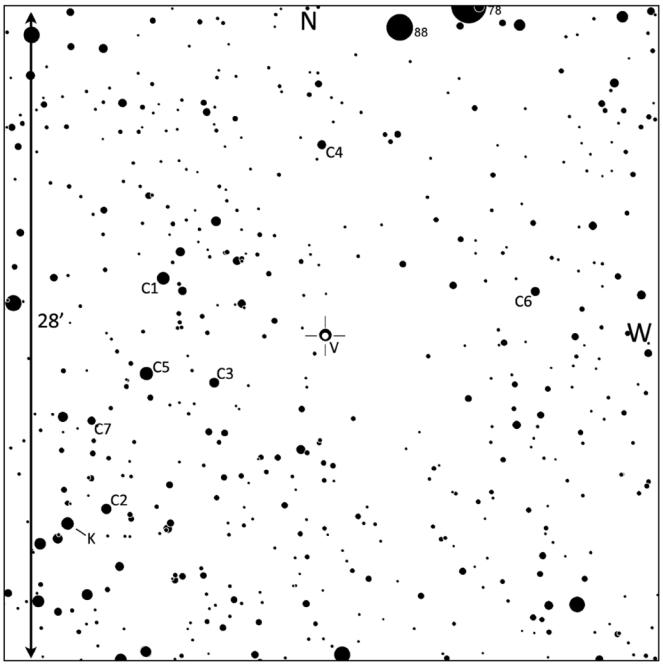

Figure 2. Finder chart for NSVS 6133550 (V), comparison (C1–C7), and check (K) stars.

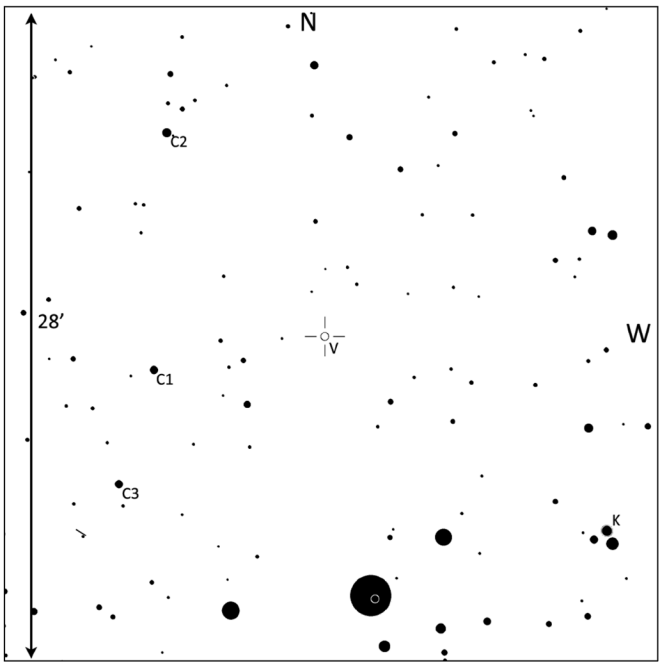

Figure 3. Finder chart for V1377 Tau (V), comparison (C1–C3), and check (K) stars.

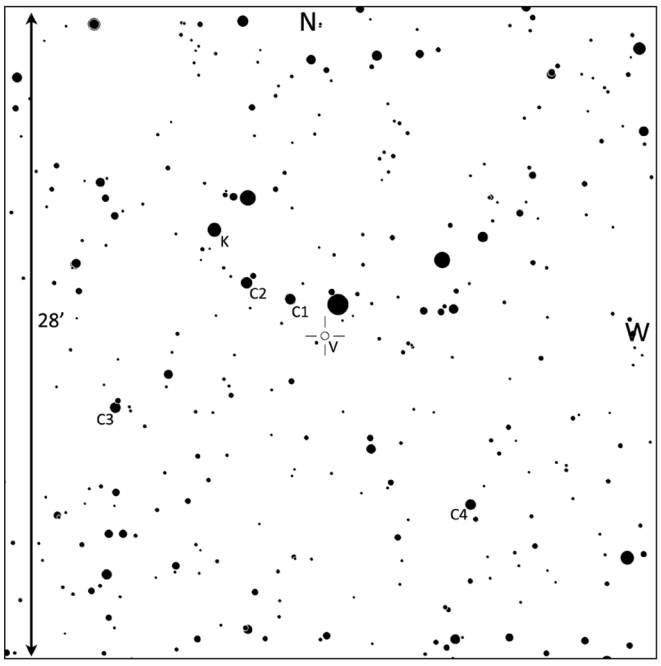

Figure 5. Finder chart for V2802 Ori (V), comparison (C1–C4), and check (K) stars.

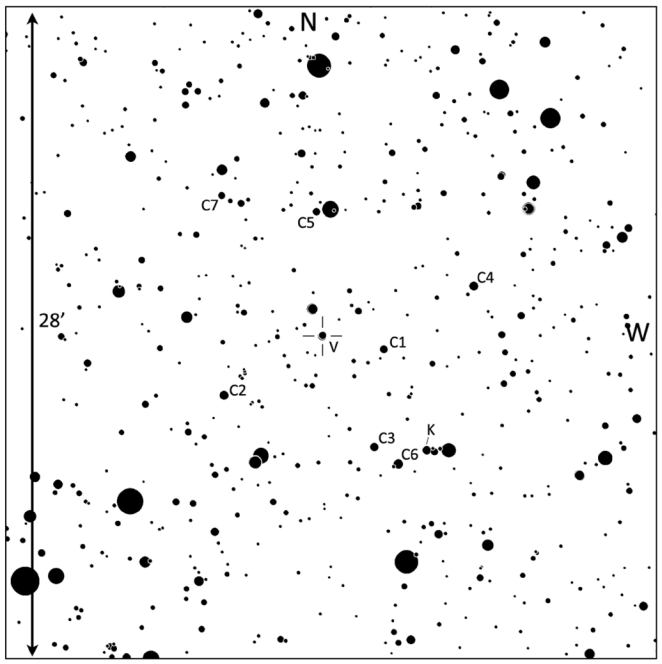

Figure 4. Finder chart for NSVS 3917713 (V), comparison (C1–C7), and check (K) stars.

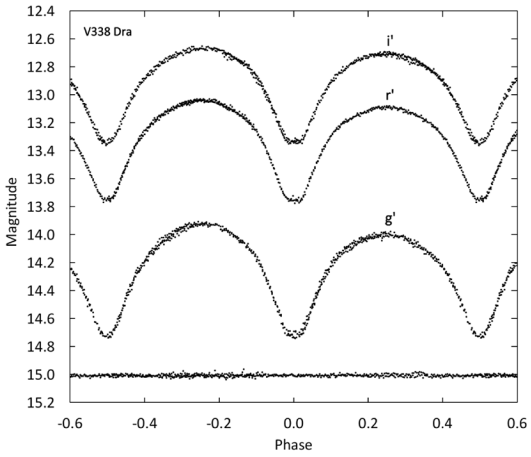

Figure 6. Observed light curves in standard magnitudes of V338 Dra (g' r' i' filters). The bottom curve shows the Sloan r' check star magnitudes (offset +1.6 magnitudes).

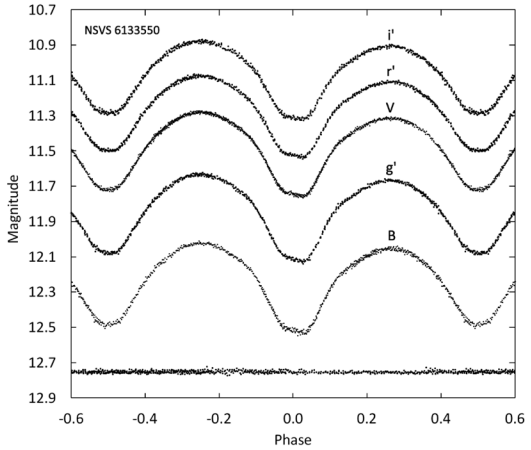

Figure 7. Observed light curves in standard magnitudes of NSVS 6133550 (B V g' r' i' filters). The bottom curve shows the Sloan r' check star magnitudes (offset +1.36 magnitudes).

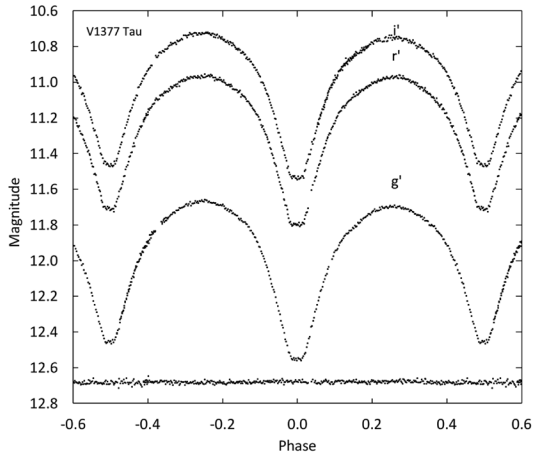

Figure 8. Observed light curves in standard magnitudes of V1377 Tau (g' r' i' filters). The bottom curve shows the Sloan r' check star magnitudes (offset +1.18 magnitudes).

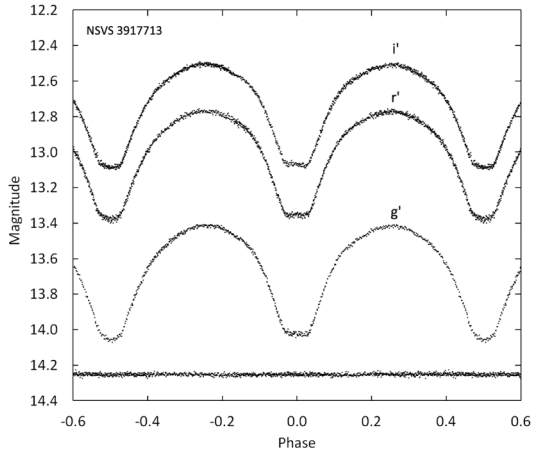

Figure 9. Observed light curves in standard magnitudes of NSVS 3917713 (g' r' i' filters). The bottom curve shows the Sloan r' check star magnitudes (offset +1.5 magnitudes).

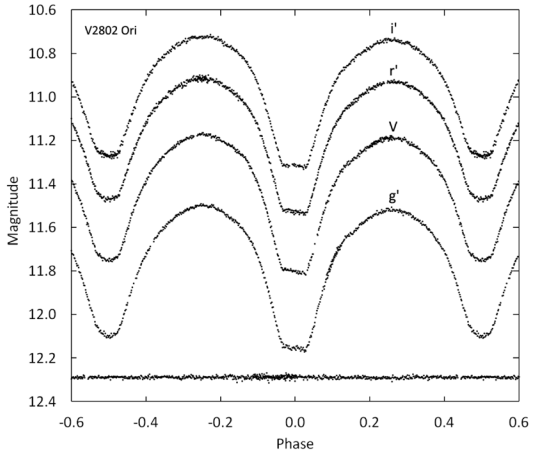

Figure 10. Observed light curves in standard magnitudes of V2802 Ori (V g' r' i' filters). The bottom curve shows the Sloan r' check star magnitudes (offset +1.5 magnitudes).

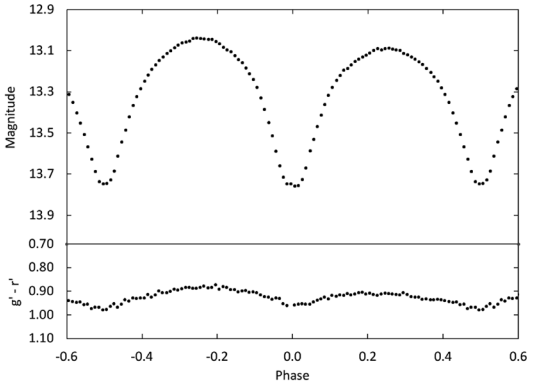

Figure 11. Light curve of all Sloan r'-band observations in standard magnitudes for V388 Dra (top panel). The observations were binned with a phase width of 0.01. The errors for each binned point are about the size of the plotted points. The g'- r' colors were calculated by subtracting the linearly interpolated binned g' magnitudes from the linearly interpolated binned r' magnitudes.

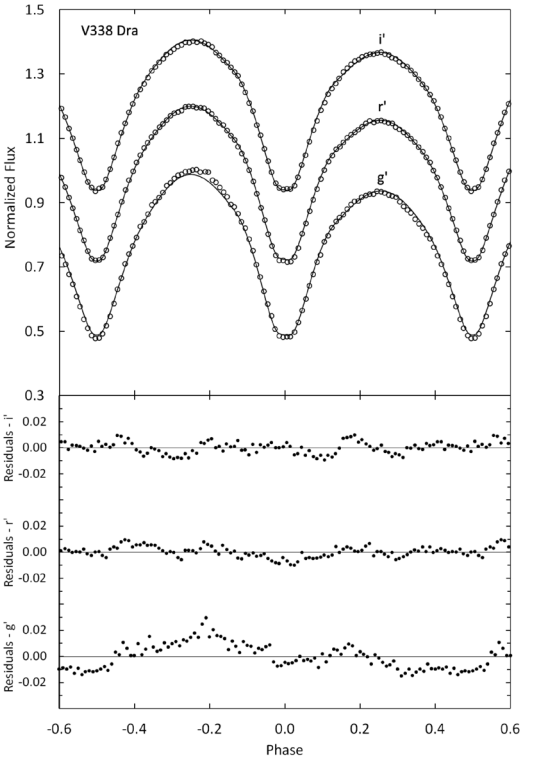

Figure 12. Comparison between the WD model fit (solid curve) and the observed normalized flux curves for V338 Dra (g' r' i' filters). Each curve is offset by 0.2 for this combined plot. The residuals for the best-fit model are shown in the bottom panel. Error bars are omitted from the points for clarity.

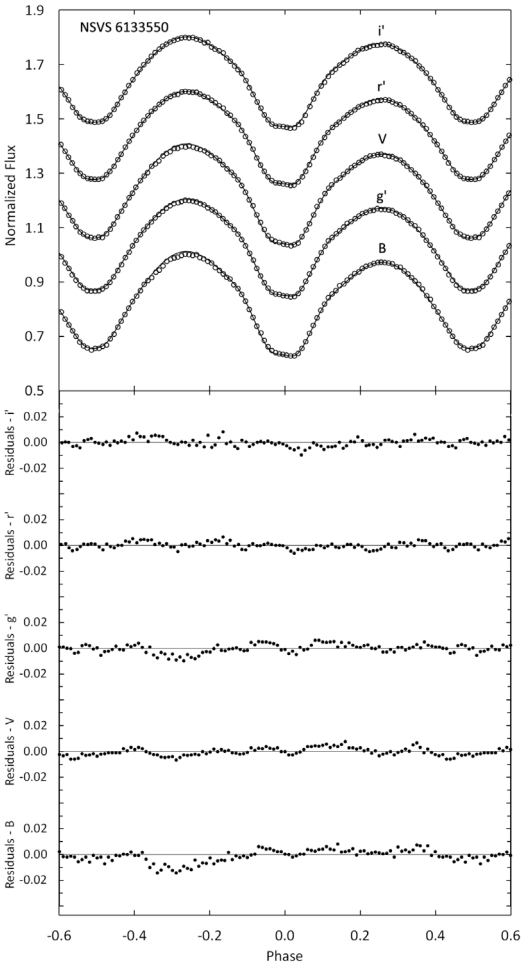

Figure 13. Comparison between the WD model fit (solid curve) and the observed normalized flux curves for NSVS 6133550 (B V g' r' i' filters). Each curve is offset by 0.2 for this combined plot. The residuals for the best-fit model are shown in the bottom panel. Error bars are omitted from the points for clarity.

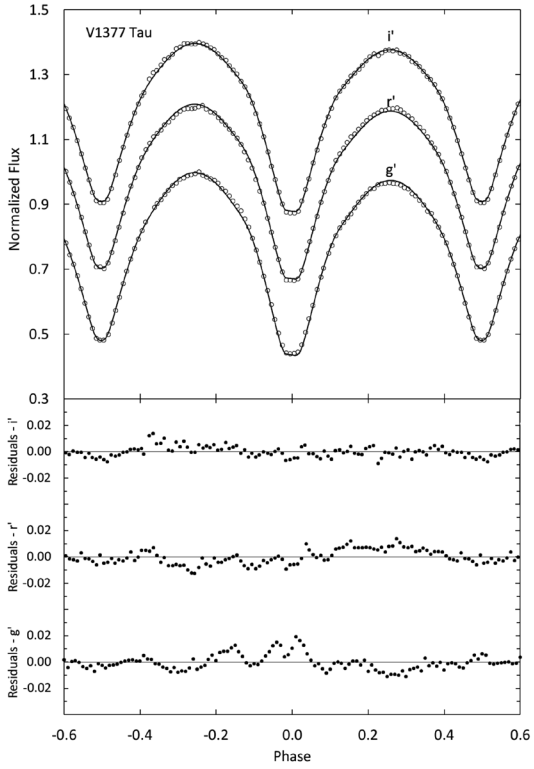

Figure 14. Comparison between the WD model fit (solid curve) and the observed normalized flux curves for V1377 Tau (g' r' i' filters). Each curve is offset by 0.2 for this combined plot. The residuals for the best-fit model are shown in the bottom panel. Error bars are omitted from the points for clarity.

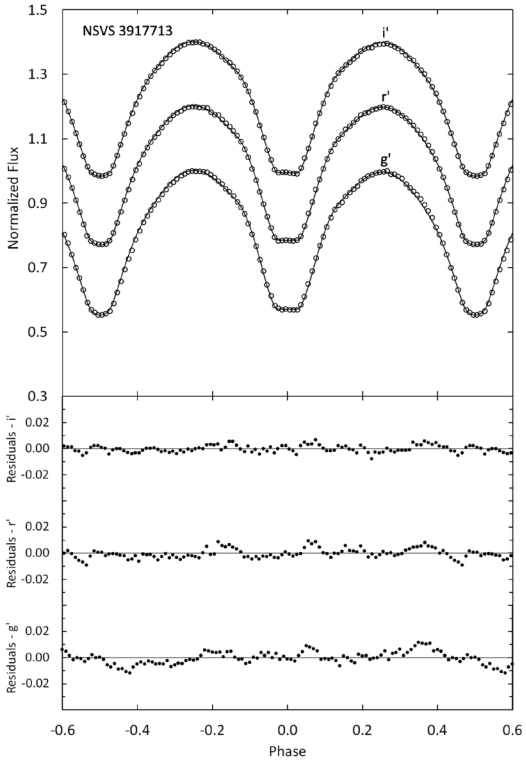

Figure 15. Comparison between the WD model fit (solid curve) and the observed normalized flux curves for NSVS 3917713 (g' r' i' filters). Each curve is offset by 0.2 for this combined plot. The residuals for the best-fit model are shown in the bottom panel. Error bars are omitted from the points for clarity.

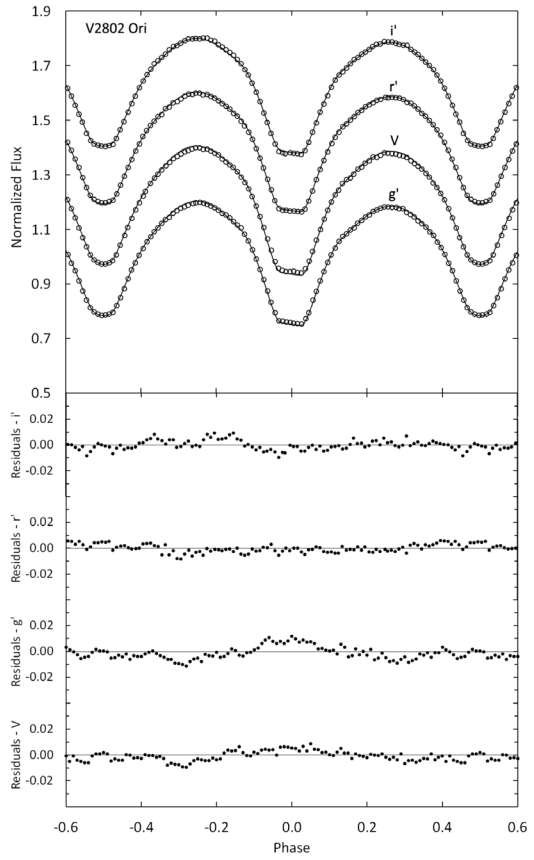

Figure 16. Comparison between the WD model fit (solid curve) and the observed normalized flux curves for V2802 Ori (V g' r' i' filters). Each curve is offset by 0.2 for this combined plot. The residuals for the best-fit model are shown in the bottom panel. Error bars are omitted from the points for clarity.

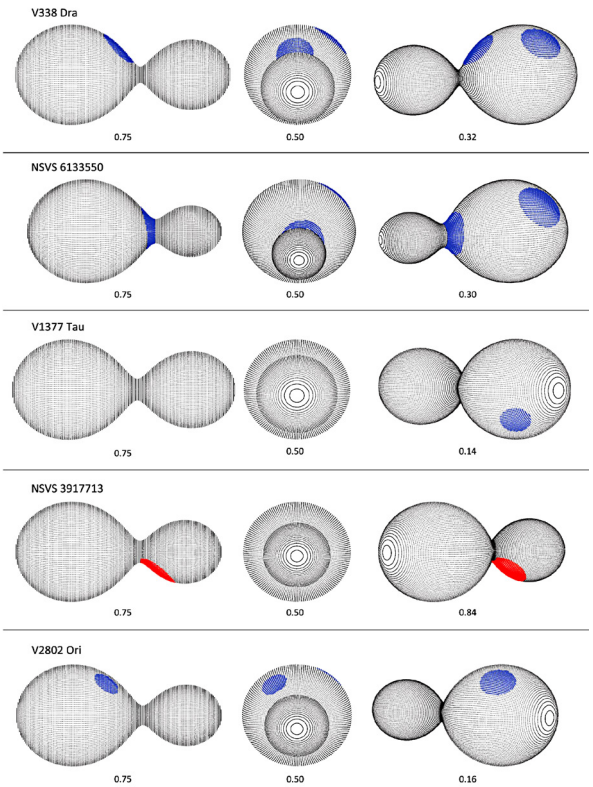

Figure 17. Roche Lobe surfaces of the best-fit WD spot model showing spot locations. The orbital phase is shown below each diagram.

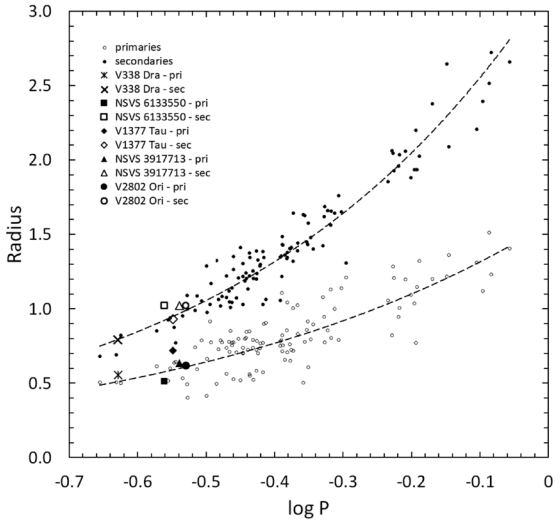

Figure 18. The radii of the stars in this study are compared with the radius distributions of 112 contact binaries with well determined geometrical and physical properties. The dashed lines are the least-square fits from the analysis of Gazeas and Stępień (2008).

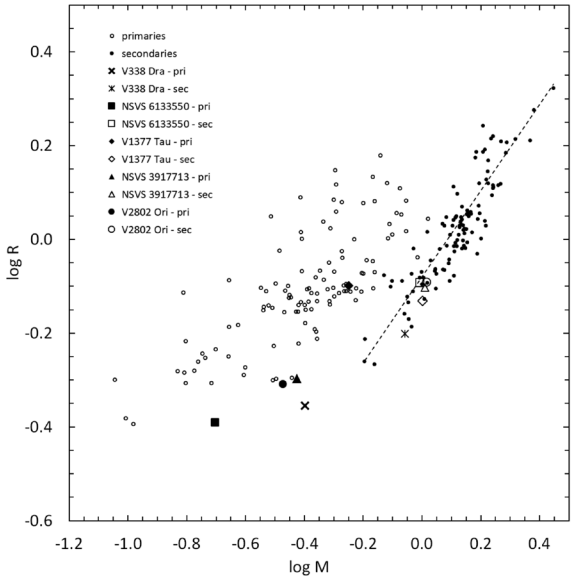

Figure 19. The radius distribution versus mass for the primary and secondary components of 112 contact binaries with well determined geometrical and physical properties. The stars in this study are shown for comparison. The dashed line is the mass-radius relation for the secondary components of contact binaries (Gazeas and Stępień 2008).

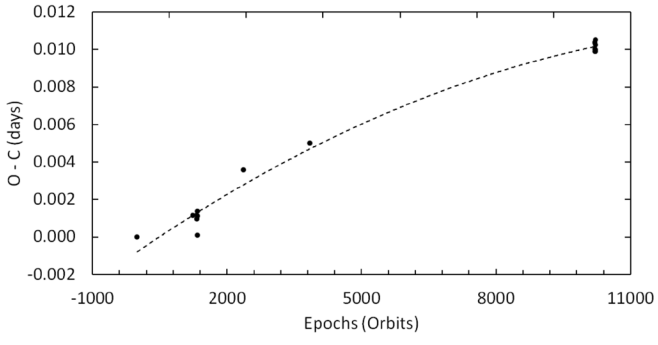

Figure 20. The O–C residuals (dots) from the initial ephemeris of V1377 Tau. The solid line is the quadratic ephemeris fit of Equation 7.